

Generating random walks and polygons with stiffness in confinement

This content has been downloaded from IOPscience. Please scroll down to see the full text.

2015 J. Phys. A: Math. Theor. 48 095202

(<http://iopscience.iop.org/1751-8121/48/9/095202>)

View [the table of contents for this issue](#), or go to the [journal homepage](#) for more

Download details:

IP Address: 152.15.112.214

This content was downloaded on 05/02/2015 at 15:44

Please note that [terms and conditions apply](#).

Generating random walks and polygons with stiffness in confinement

Y Diao^{1,5}, C Ernst², S Saarinen³ and U Ziegler⁴

¹ Department of Mathematics and Statistics, University of North Carolina Charlotte, Charlotte, NC 28223, USA

² Department of Mathematics, Western Kentucky University, Bowling Green, KY 42101, USA

³ Department of Mathematics, University of Kentucky Lexington, KY 40526, USA

⁴ Department of Computer Science, Western Kentucky University, Bowling Green, KY 42101, USA

E-mail: YuananDiao@uncc.edu

Received 29 October 2014

Accepted for publication 28 November 2014

Published 4 February 2015



CrossMark

Abstract

The purpose of this paper is to explore ways to generate random walks and polygons in confinement with a bias toward stiffness. Here the stiffness refers to the curvature angle between two consecutive edges along the random walk or polygon. The stiffer the walk (polygon), the smaller this angle on average. Thus random walks and polygons with an elevated stiffness have lower than expected curvatures. The authors introduced and studied several generation algorithms with a stiffness parameter $s > 0$ that regulates the expected curvature angle at a given vertex in which the random walks and polygons are generated one edge at a time using conditional probability density functions. Our generating algorithms also allow the generation of unconfined random walks and polygons with any desired mean curvature angle. In the case of random walks and polygons confined in a sphere of fixed radius, we observe that, as expected, stiff random walks or polygons are more likely to be close to the confinement boundary. The methods developed here require that the random walks and random polygons be rooted at the center of the confinement sphere.

Keywords: random walks, random polygons, confinement, stiff random walks, stiff random polygons

(Some figures may appear in colour only in the online journal)

⁵ Author to whom any correspondence should be addressed.

1. Introduction

It is well known the packing of genomic material (long DNA chains) inside living organisms can be highly compact. For example, even in the case of a simple organism such as the P4 bacteriophage virus, the DNA packing is of high density: its $3\ \mu\text{m}$ long double-stranded DNA is packed within a bacteriophage head capsid with a caliper size of about 50 nm, corresponding to a 70-fold linear compaction [10]. Understanding how DNA is packed under these extreme conditions is a very important yet difficult problem in molecular biology. It has been suggested that the topological information of the DNA packed inside a tight volume such as a bacteriophage head capsid can be used as a probe in studying the packing mechanism of the DNA [1]. Indeed, the topological information obtained from the circular DNA extracted from a phage head capsid revealed a high percentage of complicated knots and a lack of certain chiral knots [1]. Such information can be used to refute or support a DNA packing model for the bacteriophage. For example, in [11] Marenduzzo *et al* used semiflexible chains of beads as models of DNA to demonstrate that DNA–DNA interactions may be responsible for the DNA knotting patterns observed in bacteriophage capsids reported in [1].

In [6, 7, 9] the authors introduced models of equilateral random polygons in spherical confinement as well as algorithms for generating these random polygons. One motivation for studying a confined equilateral random polygon model is the above DNA packing problem and more generally the study of the properties of long polymer chains subject to a tight confinement condition. Here, confined random walks and polygons (and their variations) provide a modeling tool in understanding and analyzing such problems numerically. In general, a random walk with certain bending rigidity at the vertices (also called a wormlike chain) is more preferable in modeling objects such as polymer or DNA chains due to their local rigidity. This brings in the problem of how to generate confined equilateral random walks and polygons. Without any additional restrictions, an equilateral random walk has an average curvature angle of $\pi/2$ at each vertex, while an equilateral random polygon has a slightly larger average curvature angle at each vertex due to the closed curve effect [15]. Usually, a *stiff* random walk or polygon simply refers to a random walk or polygon that has a lower average curvature when compared to the unconditioned random walks and polygons. When generating a random walk or polygon confined in a tight volume without considering the stiffness factor, the volume constraint forces the random walks and polygons to bend more. This is rather intuitive and is indeed observed in [8]. Thus the random walks and polygons generated using methods from [6, 7, 9] are not good candidates to model polymer chains or DNA chains that have natural stiffness since they behave very differently in terms of their geometric and topological properties than random walks and polygons with added stiffness.

Unfortunately, it is not an easy task to generate confined random walks and polygons even without the added stiffness as the authors had demonstrated in their earlier work [6, 7, 9]. To the knowledge of the authors, there are no known theoretical probability distributions of equilateral random polygons with added stiffness and confinement. Instead, random walks are usually used and various closure schemes are used to measure the knot-tiness of the random walks generated. See for example [12–14].

In this paper the authors study the generation of confined equilateral random walks and polygons with a bias toward higher degree of stiffness. The main approach used in this paper is to modify the generation methods introduced in [6, 7, 9], which rely on the use of explicit probability density functions that guide the generation of the polygons in an edge-by-edge manner, to include a parameter that controls the stiffness of the random walks and polygons generated. We demonstrate that, depending on the local curvature bias used, different stiff random walks and polygons can be generated even though they may share the same overall

mean total curvature. In other words, there are many different ways to model confined or unconfined random walks and polygons with stiffness.

We should point out that our approaches and results are rather theoretical (mathematical). Although our work is motivated by the DNA packing problem, we do not claim that the random walks or polygons generated by our algorithms are realistic confined DNA or polymer chain models. Our intention is only to demonstrate a few approaches on how to introduce an elevated stiffness in a random walk or random polygon where the degree of stiffness may be controlled by a parameter. A seemingly setback of our results is that our generation methods require that the random walks and polygons be rooted at the center of the confining sphere, which is a strong and artificial condition. However, this paper introduces the first attempts on adding stiffness to random walks and polygons and some progress has been made. We should also point out that recently, using a very different approach to generate random polygons, J Cantarella *et al* have also proposed a fast algorithm to generate confined equilateral random polygons [2–4], though it is unclear how suitable it is to introduce an additional stiffness parameter in that model.

The paper is organized as follows: In section 2 we first study the case of stiff random walks without confinement. A few examples are discussed and compared. In section 3 we introduce confinement to our model of random walks. In section 4 we analyze how to use such schemas to generate stiff random polygons. Section 5 contains examples of generated confined random walks and polygons and finally section 6 concludes the paper with some open questions.

2. Unconfined random walks with a stiffness parameter

In this section, we use three different examples to demonstrate how a ‘stiffness parameter’ defined locally at the vertices of a random walk leads to a random walk with an overall elevated stiffness. Furthermore, we demonstrate that the parameter can be chosen to achieve a predetermined mean total curvature for the random walks generated. Consider a standard equilateral random walk W_k of length k . Let X_0, X_1, \dots, X_k be the (consecutive) vertices of the random walk defined as a Markov chain where each X_{j+1} depends only on X_j in the following way: once X_j is chosen, X_{j+1} is chosen uniformly over the unit sphere centered at X_j . Such a walk can be generated in the following way. Imagine that you have generated X_j in a walk and are looking to generate X_{j+1} on the unit sphere centered at X_j . Now on this sphere, there are circles of constant curvature (that is with a constant angle $\theta = \angle X_{j-1}X_jX_{j+1}$), and these circles are perpendicular to the previous segment $X_{j-1}X_j$. It can be demonstrated that if we select a value for $\cos(\theta) \in [-1, 1]$ with uniform probability, and then randomly choose a point on the resulting constant curvature circle, we select all points on the sphere with equal probability (for example, this fact can be found in [9]). The random walk W_k generated in this way has a mean curvature angle of $\pi/2$ with the distribution of the angle θ ranging from 0 to π given by the probability density function $\sin(\theta)/2$.

2.1. A simple cut-off model

We now modify the above to generate random walks by introducing a parameter to leverage the average curvature. As before X_j has been generated and we want to generate X_{j+1} . Here is a simple way to generate a random walk with higher stiffness. Suppose for each step in the random walk we first choose a $\tau \in [-1, 1]$ and then we choose $\cos(\theta) \in [\tau, 1]$. This is equivalent to restricting X_{j+1} to the spherical cap such that the curvature angle at X_j falls into

the interval $[0, \cos^{-1}(\tau)]$. With this approach although any curvature angle is still possible, a large curvature angle is less likely. Of course, this simple method does not control the stiffness level since it only generates one kind of random walks. So we modify it by introducing a (stiffness) parameter $s \in [0, \infty)$. As before at each step choose a value τ with uniform probability but now from the interval $[0, 1]$. Next we select $\cos(\theta)$ also with uniformly distributed probability from the interval $[1 - 2\tau^s, 1]$. Now the curvature at X_j is θ once X_{j+1} is selected on the constant curvature circle defined by θ with uniform probability. Note that if $s = 0$, then the random walk generated has no restriction on its curvature angle and we obtain the standard random walks without added stiffness (where each X_{j+1} is uniformly chosen over the unit sphere centered at X_j). For $s = 1$ we obtain the first schema we described to increase stiffness, but as $s \rightarrow \infty$, $\cos(\theta)$ is forced to be very close to 1 most of the time, creating random walks that are extremely stiff. The question is, is it possible to derive an explicit formula for the expected average curvature as a function of s ? If so then we may be able to choose the s values in order to achieve our desired average curvature values for the random walks we generate. So in the following we derive the average curvature as a function of s .

Recall that the angle θ is a random number distributed in $[0, \pi]$ such that $t = \cos \theta$ is uniformly chosen from $[1 - 2\tau^s, 1]$ while τ is itself a uniform random variable over $[0, 1]$. Thus for any given $v \in [-1, 1]$ and any fixed $\tau \in [0, 1]$, we have $P(t \leq v|\tau) = 0$ if $v \leq 1 - 2\tau^s$ (or equivalently if $\tau \leq \left(\frac{1-v}{2}\right)^{1/s}$), and $P(t \leq v|\tau) = \frac{1}{2\tau^s}(v - 1 + 2\tau^s)$ otherwise. It follows that

$$\begin{aligned} P(t \leq v) &= \int_0^1 P(t \leq v|\tau)f(\tau)d\tau \\ &= \int_{\left(\frac{1-v}{2}\right)^{1/s}}^1 \frac{1}{2\tau^s}(v - 1 + 2\tau^s)d\tau \\ &= 1 - \left(\frac{1-v}{2}\right)^{1/s} - \left(\frac{1-v}{2}\right) \int_{\left(\frac{1-v}{2}\right)^{1/s}}^1 \tau^{-s}d\tau \\ &= \begin{cases} 1 - \frac{1-v}{2} + \frac{1-v}{2} \ln\left(\frac{1-v}{2}\right), & \text{if } s = 1, \\ 1 + \frac{1-v}{2(s-1)} - \frac{s}{s-1}\left(\frac{1-v}{2}\right)^{1/s}, & \text{if } s > 0, s \neq 1, \end{cases} \end{aligned}$$

where $f(\tau) = 1$ (for $\tau \in [0, 1]$) is the probability density function of τ . For a given $\theta_0 \in [0, \pi]$, we then have

$$\begin{aligned} P(\theta \leq \theta_0) &= P(\cos \theta \geq \cos \theta_0) \\ &= 1 - P(\cos \theta \leq \cos \theta_0) \\ &= \begin{cases} \frac{1 - \cos \theta_0}{2} \left(1 - \ln \left(\frac{1 - \cos \theta_0}{2} \right) \right), & \text{if } s = 1, \\ \frac{1 - \cos \theta_0}{2(s-1)} \left(-1 + s \left(\frac{1 - \cos \theta_0}{2} \right)^{-1+1/s} \right), & \text{if } s > 0, s \neq 1. \end{cases} \end{aligned}$$

Hence $g_1(\theta, s)$, the probability density function of θ , is

$$g_1(\theta, s) = \begin{cases} \frac{-\sin \theta}{2} \ln \left(\frac{1 - \cos \theta}{2} \right), & \text{if } s = 1, \\ \frac{-\sin \theta}{2(s-1)} \left(1 - \left(\frac{1 - \cos \theta}{2} \right)^{-1+1/s} \right), & \text{if } s > 0, s \neq 1. \end{cases}$$

For $s > 0$ and $s \neq 1$, we have

$$\begin{aligned} E(\theta, s) &= \int_0^\pi \theta \cdot g_1(\theta, s) d\theta \\ &= -\frac{1}{2(s-1)} \int_0^\pi \theta \sin(\theta) \left(1 - \left(\frac{1 - \cos \theta}{2} \right)^{-1+1/s} \right) d\theta \\ &= -\frac{1}{2(s-1)} \left[\int_0^\pi \theta \sin(\theta) d\theta - \int_0^\pi \theta \sin(\theta) \left(\frac{1 - \cos \theta}{2} \right)^{-1+1/s} d\theta \right] \\ &= -\frac{1}{2(s-1)} \left[\pi - \int_0^\pi \theta \sin(\theta) \left(\frac{1 - \cos \theta}{2} \right)^{-1+1/s} d\theta \right] \\ &= -\frac{1}{2(s-1)} \left[\pi - 2s\pi + 2s \int_0^\pi \left(\frac{1 - \cos \theta}{2} \right)^{1/s} d\theta \right] \\ &= \frac{(2s-1)\pi}{2(s-1)} - \frac{s}{s-1} \int_0^\pi \left(\frac{1 - \cos \theta}{2} \right)^{1/s} d\theta \end{aligned}$$

by using integration by parts. Substituting $t = (1 - \cos \theta)/2$ in the above integral then leads to

$$\begin{aligned} E(\theta) &= \frac{(2s-1)\pi}{2(s-1)} - \frac{s}{s-1} \int_0^\pi \left(\frac{1 - \cos \theta}{2} \right)^{1/s} d\theta \\ &= \frac{(2s-1)\pi}{2(s-1)} - \frac{s}{s-1} \int_0^1 t^{\frac{1}{s}-\frac{1}{2}} (1-t)^{-\frac{1}{2}} dt \\ &= \frac{(2s-1)\pi}{2(s-1)} - \frac{s}{s-1} B\left(\frac{1}{s} + \frac{1}{2}, \frac{1}{2}\right), \end{aligned}$$

where $B(x, y)$ is the Beta function. It is known that $B(x, y)$ is related to the gamma function $\Gamma(z)$ by the identity $B(x, y) = \Gamma(x)\Gamma(y)/\Gamma(x+y)$. Thus we obtain

$$E(\theta) = \frac{(2s-1)\pi}{2(s-1)} - \frac{s\sqrt{\pi}}{s-1} \frac{\Gamma\left(\frac{1}{2} + \frac{1}{s}\right)}{\Gamma\left(1 + \frac{1}{s}\right)}.$$

For $s = 1$ the result of the integral $E(\theta) = \int_0^\pi \theta \cdot g_1(\theta) d\theta$ can be obtained directly using a software package such as Mathematica. We summarize our results in the following:

For a random walk W_k generated using the cut-off model described in the above, its expected curvature (per vertex) $E_1(W_k, s)$ is given by:

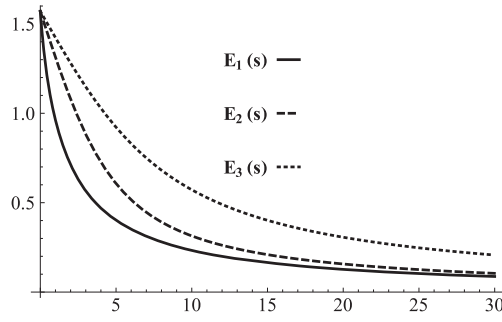


Figure 1. The expected average curvature for the three models.

$$E_1(W_k, s) = \begin{cases} \pi/2, & s = 0, \\ \pi(1 - \ln(2)), & s = 1, \\ \frac{(2s - 1)\pi}{2(s - 1)} - \frac{s\sqrt{\pi}}{s - 1} \frac{\Gamma\left(\frac{1}{2} + \frac{1}{s}\right)}{\Gamma\left(1 + \frac{1}{s}\right)}, & s > 0, s \neq 1. \end{cases}$$

The plot of $E_1(W_k, s)$ is shown in figure 1. It is a decreasing function of s with maximum $\pi/2$ at $s = 0$ and minimum 0 at $s = \infty$. Thus it is indeed possible for us to choose a suitable (and unique) s in order to generate equilateral random walks with a pre-determined average curvature value.

Of course one may use other ways to introduce a bias towards stiff random walks. In fact, a close examination of the above example shows that this method still works if we replace the density function $g_1(\theta, s)$ by any other density function. For example any non-negative continuous function $h(\theta)$ from the interval $[0, \pi]$ to \mathbb{R}_0^+ such that $\int_0^\pi h(\theta)d\theta = 1$. However, one needs to be mindful that such density functions may not produce standard equilateral random walks, even when the random walks so produced show an average curvature (per vertex) close to $\pi/2$. In the following two subsections we show two additional parametrized families that can be used to introduce a bias towards stiffness.

2.2. A simple exponential density function model

Consider the following family of functions:

$$g_2(\theta, s) = \frac{se^{s(1-\theta/\pi)}}{\pi(e^s - 1)}.$$

It is easy to see that g_2 is a probability density function for any given $s > 0$ over the domain $[0, \pi]$. We leave it to our reader to verify that the expected value for the curvature $E_2(W_k, s)$ for $s > 0$ is given by:

$$E_2(W_k, s) = \pi\left(\frac{1}{s} - \frac{1}{e^s - 1}\right).$$

We have $\lim_{s \rightarrow 0} E_2(W_k, s) = \pi/2$ and $\lim_{s \rightarrow \infty} E_2(W_k, s) = 0$, as one can easily check. However for $s = 0$, we have $\lim_{s \rightarrow 0} g_2(\theta, 0) = 1/\pi$. Recall that for the equilateral random walks without a stiffness bias, the corresponding density function for the curvature angle θ at

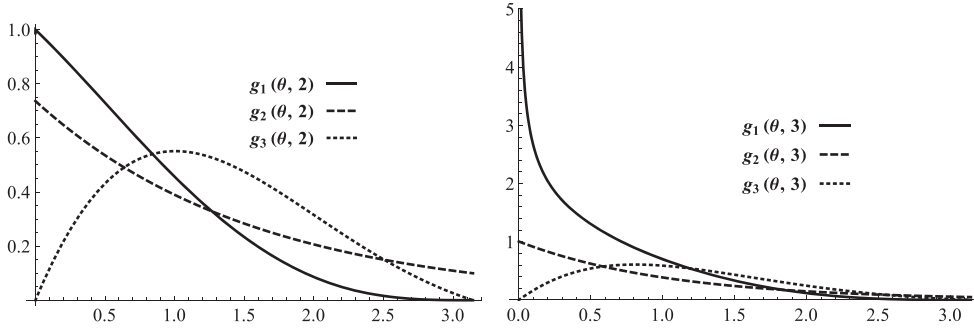


Figure 2. The probability density functions $g_1(\theta, s)$, $g_2(\theta, s)$, and $g_3(\theta, s)$ for $s = 2$ and $s = 3$.

each vertex is $\sin(\theta)/2$ (over $[0, \pi]$). Thus with this approach non-standard random walks are generated where at each step the next vertex is not chosen uniformly from the unit sphere centered at the current vertex, but instead the next vertex is chosen such that the curvature angles are uniform over $[0, \pi]$. That means very small turns and very large turns have a much higher probability of occurrence than they would normally have.

2.3. A refined exponential density function model

Here we consider the following family of functions:

$$g_3(\theta, s) = \frac{e^{s(1-\theta/\pi)}(\pi^2 + s^2) \sin(\theta)}{\pi^2(1 + e^s)}.$$

It is easy to see that these are probability density functions over the domain $[0, \pi]$. The expected value for the curvature $E_3(W_k, s)$ for $s > 0$ is given by:

$$E_3(W_k, s) = \pi \left(\frac{2s}{\pi^2 + s^2} + \frac{1}{1 + e^s} \right).$$

Again we have $\lim_{s \rightarrow 0} E_3(W_k, s) = \pi/2$ and $\lim_{s \rightarrow \infty} E_3(W_k, s) = 0$. Furthermore the function g_3 is continuous in s with $g_3(\theta, 0) = \sin(\theta)/2$. So in this case when the stiffness bias vanishes, we do get the standard equilateral random walks. The plot of $E_3(W_k, s)$, together with the plots of $E_1(W_k, s)$ and $E_2(W_k, s)$, is shown in figure 1.

2.4. Numerical comparison of the three models

From the plots of these functions in figure 1, the average curvature of random walks in all three models are strictly decreasing functions of s with $E_j(W_k, s = 0) = \pi/2$ and $\lim_{s \rightarrow \infty} E_j(W_k, s) = 0$. This common feature is what we aimed at from the beginning. Notice that their rates of decrease (as $s \rightarrow \infty$) are different. We have $\lim_{s \rightarrow \infty} \frac{E_3(W_k, s)}{E_2(W_k, s)} = 2$ and $\lim_{s \rightarrow \infty} \frac{E_1(W_k, s)}{E_2(W_k, s)} \approx 0.886294$. Also, the probability density functions used are very different. Figure 2 shows two examples of these three density functions, one for $s = 2$ and one for $s = 3$. The point is that if the only objective is to generate random walks with stiffness, then there can be many choices.

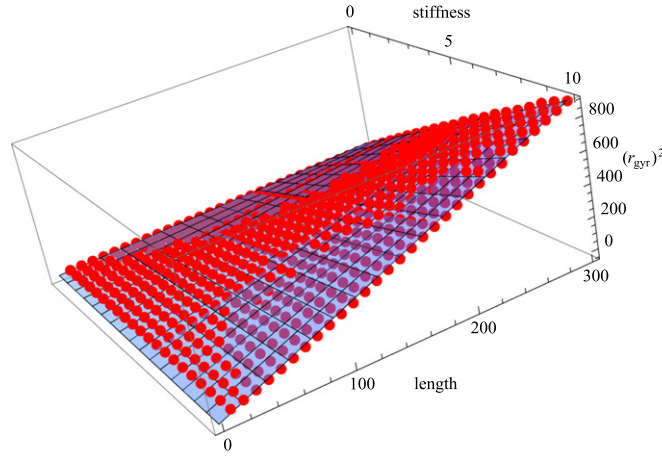


Figure 3. The effect of the stiffness parameter on the radius of gyration.

Finally, we demonstrate how the increased stiffness affects the average radius of gyration of the random walks. We only use the cut-off model here for this demonstration. Figure 3 shows the average squared radius of gyration where each data point is computed from a sample of ten thousand random walks W_k . In the figure $k \in \{10, 20, 30, \dots, 300\}$ and stiffness $s \in \{0, 1/2, 1, 3/2, \dots, 10\}$. The two variable simple best fit function $r_{\text{gyr}}^2 \approx 0.284(s+1)(k-14.017)$ yielded $r^2 \approx 0.9992$. Similar behavior is observed in the other two models.

3. Stiff equilateral random walks in confinement

Now we adapt the models in section 2 to generate a stiff random walk in confinement. We assume that we are given some probability density function of the curvature angle θ at any vertex. In this section this probability density function is simply called $g(\theta, s)$. For example, this could be any one from the three models in section 2. Let $S_R(O)$ be a confining sphere centered at the origin O with radius $R \geq 1$. Assuming that the vertices $X_0 = O, X_1, X_2, \dots, X_{k-1}, X_k$ have been generated and we need to generate X_{k+1} there are two different methods (conditions) in choosing the next vertex which were discussed in [6, 9]:

Condition (r): the next vertex X_{k+1} is generated subject to the conditions that X_0, X_1, \dots, X_{k+1} form an equilateral random walk contained within the confining sphere $S_R(O)$.

Condition (a): the next vertex X_{k+1} is generated subject to the conditions that $X_0, X_1, \dots, X_k, X_{k+1}, \dots, X_n$ form an equilateral random walk contained within the confining sphere $S_R(O)$.

The letters r and a are referring to the fact that the confining sphere acts in a way similar to a reflective surface in the first case and an absorbing surface in the second case. Both methods lead to the standard unconfined random walk when R is larger than the length of the random walk. However in the first definition, we only need to make sure that the next vertex X_{k+1} generated satisfies the condition that $|X_{k+1}| \leq R$ while in the second definition, X_{k+1} is rejected if any of the vertices X_{k+2}, \dots, X_n is not bounded in $S_R(O)$. Clearly the exact positions of $X_{k+2}, X_{k+3}, \dots, X_n$ are not known when the position of X_{k+1} is generated but different sets of potential positions for $X_{k+2}, X_{k+3}, \dots, X_n$ strongly influence the conditional probability density function that determines the position of X_{k+1} . For a more detailed discussion see [6].

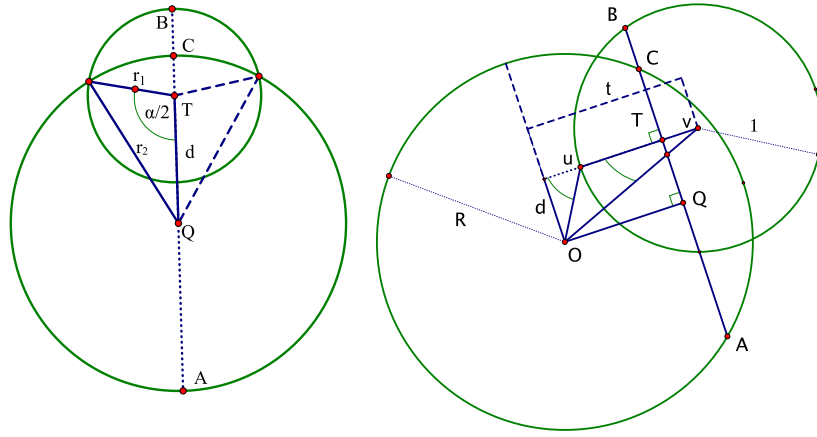


Figure 4. Left: the planar view of the circle $C_w(\theta)$ with radius r_1 in the plane P that contains it. The larger circle with radius r_2 and center Q is the intersection of P and the confinement sphere $S_R(O)$. Right: a projection into a plane perpendicular to P and containing the segment uv and the segment OQ . The intersection of the two planes contains the projection of both circles $C_w(\theta)$ and C_Q (the line segment AB in the figure). Here we see a unit circle centered at v , and a circle of radius R centered at the origin O .

In this article we only pursue condition (r) in the case of random walks to keep the involved probability density function as simple as possible. We describe a simple approach to introduce a bias toward lower curvature by scaling the given probability density function $g(\theta, s)$ of the curvature angle θ based on the portion of space available for X_{k+1} within the confinement.

Assume that $u = X_{k-1}$ and $v = X_k$ have been generated and let θ be the curvature angle at v . Let $C_w(\theta)$ be the circle on the unit sphere centered at v such that the angle between $\vec{u}\vec{v}$ and $\vec{v}\vec{z}$ is θ for any z on this circle. Thus $w = X_{k+1}$ lies on the circle $C_w(\theta)$. Let T be the center of $C_w(\theta)$ (which is not to be confused with v) and let r_1 be the radius of $C_w(\theta)$. Depending on the location of the vertices u and v the circle $C_w(\theta)$ may have a portion outside of the confinement sphere $S_R(O)$. In the case that part of $C_w(\theta)$ is outside the confinement sphere, let α be the angle of the arc of $C_w(\theta)$ contained in $S_R(O)$. The length of this arc is αr_1 .

To compute α consider a plane P containing the circle $C_w(\theta)$ (see the left of figure 4) and consider the circle C_Q which is the intersection of P and the confinement sphere $S_R(O)$. C_Q is centered at Q and has radius r_2 . The distance $\|QT\|$ is called d .

From the triangle shown in the left side of figure 4 we obtain

$$\alpha = 2 \cos^{-1} \left(\frac{d^2 + r_1^2 - r_2^2}{2r_1 d} \right),$$

and the proportion of $C_w(\theta)$ within the confinement sphere is

$$p(u, v, R, \theta) = \frac{\alpha r_1}{2\pi r_1} = \frac{1}{\pi} \cos^{-1} \left(\frac{d^2 + r_1^2 - r_2^2}{2r_1 d} \right).$$

By definition $r_1 = \sin(\theta) = \sqrt{1 - \cos^2(\theta)}$. To compute d and r_2 note that the vector \vec{OQ} is perpendicular to the plane P and so is $\vec{u}\vec{T}$ and consider a projection into the plane P' which is perpendicular to the plane P and which contains \vec{OQ} and $\vec{u}\vec{T}$ (see the right of figure 4). The

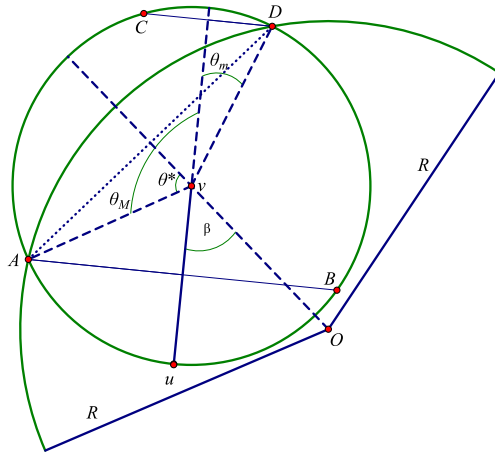


Figure 5. A planar view of the intersection of $S_1(v)$ and $S_R(O)$ on the plane defined by u, v and O . The line segment AD is the projection of the intersection circle of $S_1(v)$ and $S_R(O)$. The smallest and largest curvature angles θ_m and θ_M at the vertex v are shown together with the segments AB and CD , which are the projections of $C_w(\theta_M)$ and $C_w(\theta_m)$ respectively.

intersection of P and P' contains the projection of both circles $C_w(\theta)$ and C_Q given by the line segment \overline{AB} in the figure. $\|AB\| = \|BT\| + \|TQ\| + \|QA\| = r_1 + d + r_2 > 2r_2$. Thus when part of $C_w(\theta)$ lies outside the confinement sphere $S_R(O)$, we have $r_2 < r_1 + d$. Note that O, u , and v are never colinear if $C_w(\theta)$ is partially contained in $S_R(O)$, since colinearity would lead to concentric circles $C_w(\theta)$ and C_Q .

Since \vec{OQ} and \vec{uT} are parallel to each other d can be computed from simple geometry as $d = \|u\| \sin(\xi_1) = \|u\| \cdot \|v - u\| \sin(\xi_1) = \|u \times (v - u)\|$ (since $\|v - u\| = 1$), see figure 4 on the right. Similarly, let t be the distance shown in the right side of figure 4, then $t = \|v\| \cos(\xi_2) = v \cdot (v - u)$, and $r_2 = \sqrt{R^2 - (t + \cos(\theta))^2}$, where $\cos(\theta) = -\|TV\|$. Combining and simplifying then leads to

$$p(u, v, R, \theta) = \frac{1}{\pi} \cos^{-1} \left(\frac{d^2 + 1 - R^2 + t^2 + 2t \cos(\theta)}{2d \sin(\theta)} \right) \quad (1)$$

and this expression depends only on u, v, θ and R . In other cases $C_w(\theta)$ lies either completely inside or completely outside the confinement sphere $S_R(O)$, hence $p(u, v, R, \theta)$ either takes the value of zero or one. We need to find out when to use what. Clearly, if $\|v\| + 1 \leq R$, then $C_w(\theta)$ lies completely inside $S_R(O)$ so $p(u, v, R, \theta) = 1$. Thus we only need to consider the case $\|v\| > R - 1$ so that the unit sphere $S_1(v)$ intersects $S_R(O)$, see figure 5. As shown in the figure, in this case there exist two curvature angle values θ_m and θ_M such that if $\theta < \theta_m$, then $C_w(\theta)$ is completely outside $S_R(O)$, if $\theta > \theta_M$ then $C_w(\theta)$ is completely inside $S_R(O)$ and if $\theta_m < \theta < \theta_M$, then $C_w(\theta)$ is partly inside and partly outside $S_R(O)$. To compute the angles θ_m and θ_M let us first consider the special case when points u, v and the origin O are collinear. In this case we have the angle between \vec{vA} and \vec{Ov} is $\theta_m = \theta_M = \theta^*$ and

$$\theta^* = \cos^{-1}\left(\frac{R^2 - 1 - \|v\|^2}{2\|v\|}\right).$$

If the three points u , v and the origin O are not collinear then we can think of the segment uv as being rotated by an angle β (as shown in figure 5) around the vertex v from the collinear position. It follows that $\theta_m = |\theta^* - \beta|$ and $\theta_M = \min(\beta + \theta^*, 2\pi - (\beta + \theta^*))$, where

$$\beta = \cos^{-1}\left(\frac{(v - u) \cdot v}{\|v\|}\right).$$

Combining this with equation (1) we get (under the assumption that $\|v\| > R - 1$)

$$p(u, v, R, \theta) = \begin{cases} 0, & \theta < \theta_m, \\ \frac{1}{\pi} \cos^{-1}\left(\frac{d^2 + 1 - R^2 + t^2 + 2t \cos(\theta)}{2d \sin(\theta)}\right), & \theta_m \leq \theta \leq \theta_M, \\ 1, & \theta > \theta_M. \end{cases} \quad (2)$$

This allows us to produce an unnormalized cumulative probability density function by the following integral:

$$f(u, v, R, \theta) = \int_0^\theta g(\phi, s) \cdot p(u, v, R, \phi) d\phi. \quad (3)$$

We can then normalize $f(u, v, R, \theta)$ to obtain a cumulative probability density function for the probability:

$$F(u, v, R, \theta) = \text{Prob}(\phi \leq \theta) = \frac{f(u, v, R, \theta)}{f(u, v, R, \pi)}. \quad (4)$$

$F(u, v, R, \theta)$ is then used to generate the next vertex X_{k+1} by the following procedure. To pick the next curvature angle θ we choose a value $y \in [0, 1]$ with uniform probability and approximate $F^{-1}(u, v, R, y)$ (u, v, R are fixed here so F is an increasing function of θ) using a simple bisection method until we have obtained a curvature angle θ with a desired precision. Once the curvature angle θ is determined, we then find the circle $C_w(\theta)$ and we choose X_{k+1} uniformly from the portion of it that is inside the confinement sphere.

4. Stiff equilateral random polygons in confinement

By definition, a random polygon is a random walk conditioned on the closure, namely that the last vertex of the random walk be the same as its starting vertex. Thus, closing the random walks by a closure scheme such as those discussed in [12–14] would not generate ‘true random polygons’. The generation of a random polygon is possible, at least in theory, if the probability density distributions of the vertices of the corresponding random walks are known as the authors have demonstrated in [6, 7, 9]. Unfortunately for the random walks generated using the methods in the previous sections, theoretical probability density functions of the vertex distributions are not known and we could only estimate the probability density distributions of the vertices numerically (which we will not do in this paper due to its computational complexity). However we can force a stiff random walk to close by using any conditional probability density functions that force our standard random walks to close. The conditional probability density functions used in this section are for demonstration purposes and the stiff confined random polygons so generated are not the counterpart of the stiff

random walks generated in the earlier examples. However if the conditional probability density functions from these stiff random walks are used instead, then the generation method described in this section would at least generate the stiff random polygons with the right vertex distribution in terms of the distance of the vertex to the center of the confining sphere.

In the algorithms described in [6–9] of these algorithms a random polygon is generated one edge at a time. More specifically, if v is the last vertex generated then the next vertex w is generated by choosing $r = ||w|| \in [||v|| - 1, \min(R, |v| + 1)]$ first according to its probability density function (conditioned at the vertex v). w is then chosen uniformly on the circle $C_r(v) = S_r(O) \cap S_1(v)$. This generation process guarantees the closure of the polygon at the end and the polygon is generated according to its theoretical probability distribution. Our approach is to keep the first step of the methods in [6–9], namely to choose r first using its probability density function derived there, as this guarantees the closure of the polygon at the end. We assume that we are given a conditional probability density function $h_k(r|t)$ that describes the probability distribution of $r = ||w||$ given that (i) $t = ||v||$ and (ii) we have k steps to take before we have to arrive back at the origin in order to close the polygon. We achieve the stiffness effect by choosing first the circle $C_r(v)$ and then by choosing w on $C_r(v)$ using a probability density function $g(\theta, s)$ that favors low curvature such as those discussed in section 2.

Recall that $p(u, v, R, \theta)$ is the proportion of $C_w(\theta)$ that is within the confining sphere. If we replace R by r , then $p(u, v, r, \theta)$ gives the proportion of $C_w(\theta)$ within the sphere $S_r(O)$. For the confined random walks, the rescaling approach used in the last section leads to

$$\text{Prob}(|w| \leq r | u, v) = P_w(r) = \int_0^\pi g(\theta, s) \cdot p(u, v, r, \theta) d\theta. \tag{5}$$

$P_w(r)$ is a cumulative probability density function in the variable r , i.e. $P_w(r) = 0$ for $r \leq ||v| - 1|$ and $P_w(r) = 1$ for $r \geq |v| + 1$. The purpose of deriving $P_w(r)$ is so that we can use $P'_w(r)$ to rescale the probability density function of w as a vertex of a confined random polygon. More precisely, assume that there are k vertices left in the polygon to be generated and let $h_k(r|t)$ be the conditional probability density of w conditioned on $||v|| = t, ||w|| \leq R$ and that the polygon is to be closed in k steps. Then we define the rescaled probability density function of w by

$$h_{k,s}^*(r|t) = \frac{1}{a(k, t)} P'_w(r) h_k(r|t),$$

where

$$a(k, t) = \int_I P'_w(r) h_k(r|t) dr,$$

is the re-normalization constant and $I = [||v|| - 1, \min(R, |v| + 1)]$. $h_{k,s}^*(r|t)$ is now a probability density function that given a current position $||v|| = t$, the previous position u , a stiffness parameter s , and the number k of steps left before returning to the origin allows us to choose the circle $C_r(v)$ as the set of possible locations of w . Of course, in order to do this we need to integrate $h_{k,s}^*(r|t)$ to obtain the cumulative probability density function to be used for an inverse look-up by a bisection method. Due to the complexity of the integrals involved these computations can only be done numerically.

There are several steps involved in deriving a probability distribution for correctly choosing the θ to pick w on $C_r(v)$. First we need to modify $g(\theta, s)$ to account for the fact that for every θ there are now at most two points on $C_r(v)$ with a fixed curvature as opposed to circles of varying sizes on the unit sphere. Second, we need to determine the probability

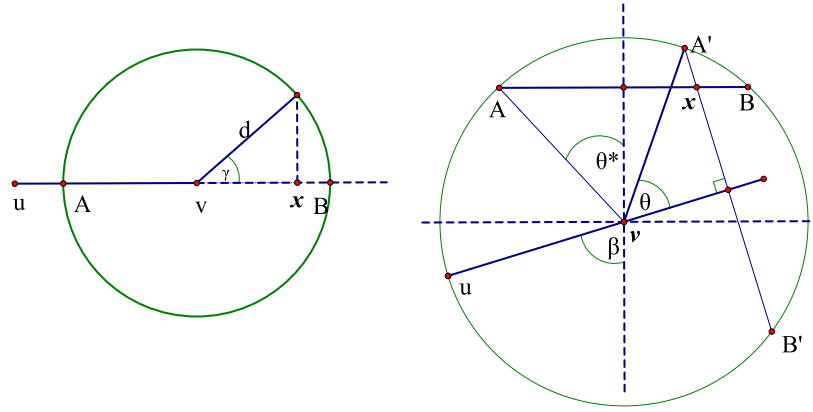


Figure 6. On the left a projection of the circle $C_r(v)$ into the plane perpendicular to \vec{Ov} . The points A, B correspond $\cos(\theta_M)$ and $\cos(\theta_m)$ respectively. On the right, the plane normal to the circles $C_r(v)$ (projected to \overline{AB}) and $C_w(\theta)$ (projected to $\overline{A'B'}$). The projection onto the plane is selected to set up a coordinate system indicated by the dashed lines: v is at $\{0, 0\}$ and the origin is on the negative y -axis. The detailed derivation in the text assumes that u is to the left of v .

density function for the curvature angle θ over the points on $C_r(v)$. And third, we need to determine the range of possible θ s for the given u, v , and $C_r(v)$. Each of these is addressed separately in the following paragraphs.

First we need to generate w on $C_r(v)$ with the same distribution as if we had randomly sampled points according to the stiffness probability density function $g(\theta, s)$ (restricted to only those points that lie on $C_r(v)$). If we were to sample points on the unit sphere $S_1(v)$ with uniform probability using spherical coordinates (θ, ϕ) where θ is the curvature angle and ϕ is an angle that is uniformly chosen in $[0, 2\pi)$ and were to select a specific point from the circle of points resulting in a fixed constant curvature θ then the size of that circle changes proportional to its radius $\sin(\theta)$. To adjust $g(\theta, s)$ so that it reflects the probability distribution of curvatures represented along the circle $C_r(v)$, we divide it by $\sin(\theta)$ and renormalize to obtain

$$p_c(\theta) = g(\theta, s) \cdot \frac{1}{\sin(\theta)} \cdot \frac{1}{b},$$

where $b = \int_0^\pi g(\theta, s) \cdot \frac{1}{\sin(\theta)} d\theta$ is the normalizing constant.

Second, to represent the relative availability of points with given curvature along the circle $C_r(v)$, we need to determine how the probability distribution for θ changes with a point x moving from B to A on the projection of $C_r(v)$, see figure 6 for the a visual display of the various variables we will be using. Let x be a given point on \overline{AB} as shown in figure 6 (on the right and the left). For the determination of x we pick a projection such that $v = \{0, 0\}$ and O is on the negative y -axis. Simple geometry leads to $r_c = \sin(\theta^*)$ and $x = r_c \cos(\gamma)$ where by a slight abuse of notation $|x|$ represents the distance from v to x as shown in figure 6 on the left or the distance from the y -axis to x along the line segment AB in figure 6 on the right. The angle marked β in this figure 6 is the same as in figure 5 which was computed in the previous section as $\beta = \cos^{-1}\left(\frac{(v-u) \cdot v}{\|v\|^2}\right)$. θ^* is also the same as in figure 5, except we use r instead of R to compute is as $\theta^* = \cos^{-1}\left(\frac{r^2 - 1 - \|v\|^2}{2\|v\|}\right)$.

We now have

$$\text{Prob}(\phi \leq \theta) = \text{Prob}(\phi \leq \gamma) = \frac{2\gamma r_c}{2\pi r_c} = \frac{\gamma}{\pi} = \frac{1}{\pi} \cos^{-1}\left(\frac{x}{r_c}\right).$$

To express x in terms of $u, v, r,$ and θ we determine x as the intersection of the projection of $S_r(v)$ and $C_v(\theta)$ which are the line segments \overline{AB} and $\overline{A'B'}$ in figure 6 on the right which shows a plane which is perpendicular to $C_r(v)$ and contains $u, v,$ and O . If u is to the left of v and $\beta \neq \pi/2$ then the slope of the line going through (A', B') is $-\tan(\beta)$. (This follows from the fact that the slope of the line through u and v is $\cot(\beta)$.) The coordinates of the point A' are $(\sin(\pi - \beta + \theta), -\cos(\pi - \beta + \theta)) = (\sin(\beta - \theta), \cos(\beta - \theta))$. Thus the line through A' and B' has equation $y = -\tan(\beta)x + \tan(\beta)\sin(\beta - \theta) + \cos(\beta - \theta)$. The equation of the line \overline{AB} representing the projection of the circle $C_r(v)$ is $y = \cos(\theta^*)$. Solving for x results in

$$x = \cot(\beta) \left(\tan(\beta)\sin(\beta - \theta) + \cos(\beta - \theta) - \cos(\theta^*) \right).$$

Substituting this in for x gives us

$$\text{Prob}(\phi \leq \theta) = \frac{1}{\pi} \cos^{-1} \left(\frac{\cot(\beta) \left(\tan(\beta)\sin(\beta - \theta) + \cos(\beta - \theta) - \cos(\theta^*) \right)}{r_c} \right).$$

Taking the derivative and simplifying we obtain a (non-normalized) probability density function p^c for θ on $C_r(v)$

$$p^c(\theta) = \frac{\sin(\theta)}{\pi \sqrt{\sin^2(\beta)\sin^2(\theta^*) - \left(\cos(\beta)\cos(\theta^*) - \cos(\theta)\right)^2}}.$$

If $\beta = \pi/2$ then $x = \sin(\beta - \theta) = \cos(\theta)$. Taking the derivative of $\frac{1}{\pi} \cos^{-1}\left(\frac{x}{r_c}\right)$ leads to and $p^c(\theta) = \frac{\sin(\theta)}{\pi \sqrt{\sin^2(\theta^*) - \cos^2(\theta)}}$ which is the same as the above, if β is replaced by $\frac{\pi}{2}$.

We now scale the adjusted stiffness pdf by the availability of points to get the probability distribution for curvatures at a given next radius.

$$P(\theta|v, u, r) = \begin{cases} p_c(\theta) \cdot p^c(\theta), & \text{if } \theta_m \leq \theta \leq \theta_M, \\ 0, & \text{if } 0 < \theta < \theta_m \text{ or } \theta_M < \theta \leq \pi, \end{cases}$$

where θ_m is the value of θ when x is at B in figure 6 and θ_M is the value of θ when x is at A . Integrating and normalizing gives us a cumulative probability density function that allows us to choose a curvature $\theta \in [\theta_m, \theta_M]$ that can occur on $C_r(v)$.

$$\text{Prob}(\phi \leq \theta) = \frac{\int_{\theta_m}^{\theta} P(\phi|v, u, r) d\phi}{\int_{\theta_m}^{\theta_M} P(\phi|v, u, r) d\phi}.$$

Notice that if $\theta \neq \theta_m, \theta_M$, there are two points on $C_r(v)$ which satisfy the radius and curvature conditions, and we may uniformly choose one of them.

This only leaves the determination of the range of possible θ associated with a given r . θ_m is the smallest θ which results in a point on $C_r(v)$ and is the angle between $\vec{u}\vec{v}$ and $\vec{v}\vec{B}$ in the projection of $C_r(v)$. Similarly, θ_M is the largest θ which results in a point on $C_r(v)$ and is the

angle between $\vec{u}v$ and $\vec{v}A$ in the projection of $C_r(v)$. Using the β and θ^* computed earlier we have

$$\theta_m = |\beta - \theta^*| = \begin{cases} \theta^* - \beta, & \text{if } \|2v - u\| > r, \\ \beta - \theta^*, & \text{if } \|2v - u\| \leq r, \end{cases}$$

and

$$\theta_M = \beta + \theta^* = \begin{cases} 2\pi - (\beta + \theta^*), & \text{if } \beta + \theta^* > \pi, \\ \beta + \theta^*, & \text{if } \beta + \theta^* \leq \pi. \end{cases}$$

Note that θ_m and θ_M only depend on u , v , and r which are all available after r has been picked.

A similar derivation for the case that u is to the right of v results in a sign change for x and $p^c(\theta)$ and finally to the same results for θ_m and θ_M and $\text{Prob}(\phi \leq \theta)$.

The above discussion works for u to the left or the right of v , but not if u , v and O are co-linear. Remember that if u , v , and O are co-linear, and $r \in I$ then the circle $C_w(\theta)$ of constant curvature θ and the intersection circle $C_r(v)$ of constant given distance r from the origin are concentric circles. Furthermore, they are identical for $\theta_0 = \cos^{-1}\left(\frac{r^2 - 1 - \|v\|^2}{2\|v\|}\right)$. For θ larger (smaller) than this computed threshold θ_0 , $C_w(\theta)$ is completely inside (outside) $S_r(v)$ and for θ smaller (larger) θ_0 , $C_w(\theta)$ is completely outside (inside) $S_r(v)$ if $\|Ou\|$ is smaller (larger) than $\|Ov\|$. Thus equation (5) simplifies to

$$P_w(r) = \begin{cases} \int_{\theta_0}^{\pi} g(\theta, s) d\theta, & \text{if } \|Ou\| \leq \|Ov\|, \\ \int_0^{\theta_0} g(\theta, s) d\theta, & \text{if } \|Ou\| > \|Ov\|. \end{cases}$$

We adjust and rescale $P_w(r)$ to obtain a probability density function $h_{k,s}^*(r|t)$ to pick the next r as before and then randomly pick a point from the resulting circle of intersection $S_r(v)$, since all points on it have constant curvature.

5. The effect of stiffness on the geometry of random walks and polygons

5.1. Random walks

Intuitively, we expect the effect of stiffness in confinement to push the random walk towards the boundary. If we consider three consecutive vertices of a walk along the boundary of the confinement sphere then the curvature angle of $2 \sin^{-1}(1/(2R))$ depends only on the confinement radius R . We expect the mean curvature of the random walk to converge to this value as the stiffness increases. figure 7 shows this effect for the refined exponential model and figure 8 shows the effect of confinement on the distribution of the curvature angle for the cut-off model. The blue curve shows the theoretical angle distribution function without confinement. This shows that the confinement shifts the angle distribution towards larger angles. Finally, figure 9 shows the effect of confinement on the distribution of vertices for the refined exponential model. The blue curve for $s = 0$ shows the theoretical vertex distribution of the random walk in confinement. This shows that the increasing stiffness pushes the vertices towards the boundary of the confinement sphere.

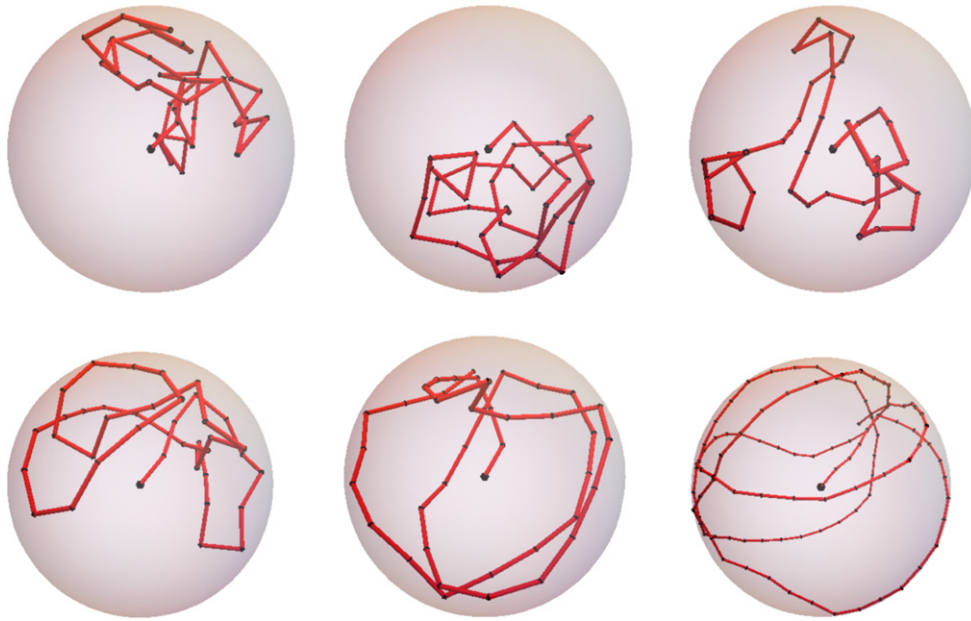


Figure 7. Examples of six random walks of length 40 using the refined exponential model with stiffness values $s = 1, 2, 4, 8, 16$ in a sphere with radius of confinement $R = 3$. The walk on the bottom right has length 100, stiffness $S = 32$ and radius of confinement $R = 5$.

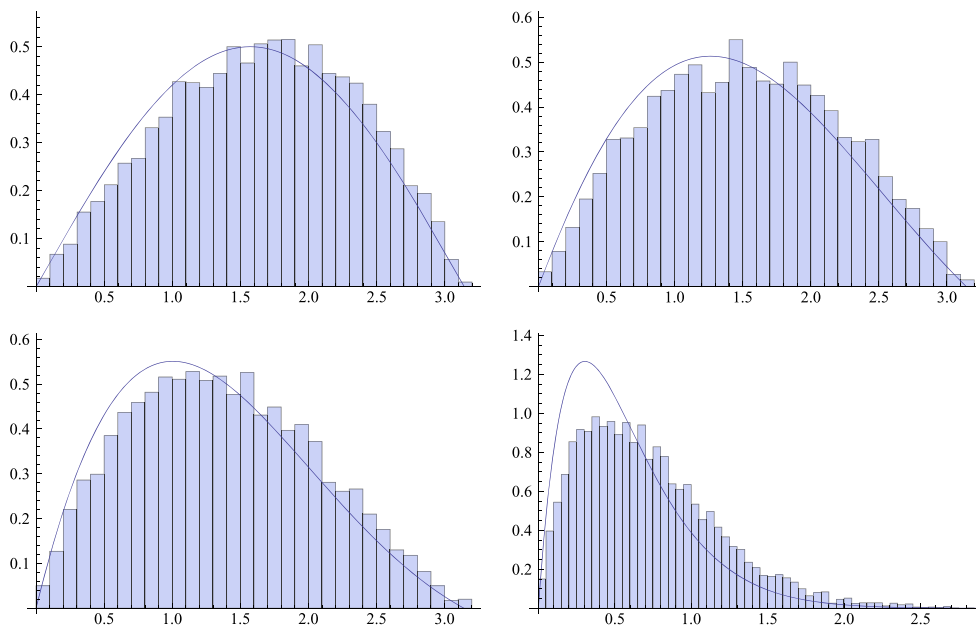


Figure 8. Examples of the angle distribution using the cut-off model with stiffness values $s = 0, 1, 2, 10$. The radius of confinement is $R = 3$. Each example is based on a random walk of length ten thousand steps.

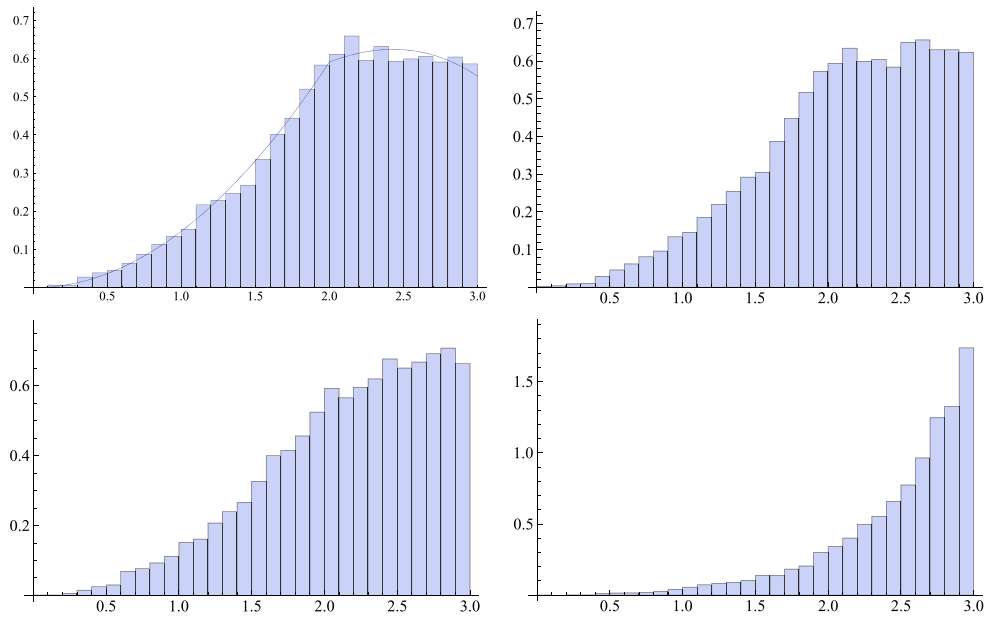


Figure 9. Examples of the vertex distribution using the refined exponential model with stiffness values $s = 0, 1, 2, 10$. The radius of confinement is $R = 3$. Each example is based on a random walk of length ten thousand steps.

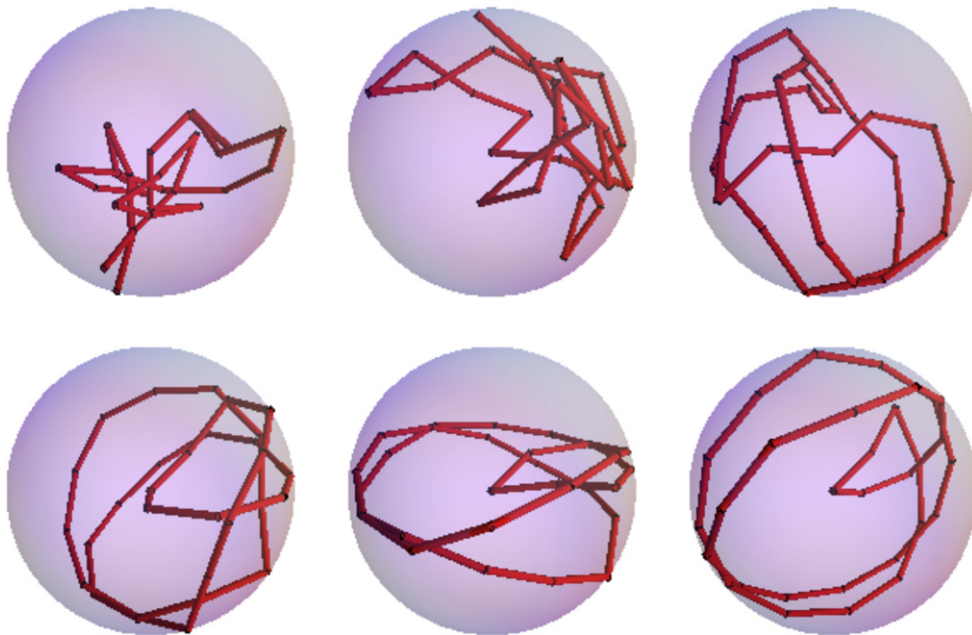


Figure 10. Examples of six random polygons of length 30 using the refined exponential model with stiffness values $s = 1, 4, 8, 16, 32$ and 64 . The radius of confinement is $R = 2$.

5.2. Random polygons

Just as in the case for random walks, we expect the effect of stiffness in confinement to push the random polygon towards the boundary. Figure 10 shows this effect for the refined exponential model using the volume functions of [6] for the polygon generation. The random polygons have length 30 and are in a confinement sphere of radius 2. We can clearly spot the origin where the polygons are rooted for stiffer polygons with s values of up to $s = 64$. Unfortunately our method does not allow us to control the curvature angle at the root of the polygon.

6. Conclusions and open questions

Following our earlier methods [6–9], we explored in this paper the generating method of equilateral random walks and polygons confined within a sphere (and rooted at the center of the polygon) with a stiffness parameter that can be chosen by the user. We showed how the stiffness affects the shape of walks and polygons. Many questions remain to be answered. For example, the polygons are rooted at the center of the confining sphere which generates a vertex with a potentially very large curvature angle. Can our algorithms be modified to avoid this problem? The algorithms presented here have a relatively large run time, is it possible to speed up the calculations? Finally, in [5] the authors study the knot spectrum of random polygons in confinement to address questions like the following: How fast does confinement increase the probability of knotting? What types of knots appear in confined polygons? The methods in this paper will allow us to also study the question: How does stiffness affect the probability of knotting? What is the effect of stiffness on the knot types of stiff random polygons? Finally, we can ask if the knot types of stiff polygons match the knot types observed experimentally in [1]. (It is known that the knot types observed without a stiffness parameter do not match the experimental results [5].) These are a few directions that we intend to pursue in the future.

Acknowledgments

Y Diao was supported in part by NSF Grants #DMS-0920880, #DMS-1016460 and by Chinese NSF grant 91324201, C Ernst, S Saarinen and U Ziegler were supported in part by NSF grant #DMS-1016420.

References

- [1] Arsuaga J, Vazquez M, McGuirk P, Trigueros S, Sumners D W and Roca J 2005 DNA knots reveal a chiral organization of DNA in phage capsids *Proc. Natl Acad. Sci. USA* **102** 9165–9
- [2] Cantarella J, Deguchi T and Shonkwiler C 2013 Probability theory of random polygons from the quaternionic viewpoint *Commun. Pure Appl. Math.* **67** 1658–99
- [3] Cantarella J, Grosberg A Y, Kusner R B and Shonkwiler C 2012 The expected total curvature of random polygons arXiv:1210.6537
- [4] Cantarella J and Shonkwiler C 2013 The symplectic geometry of closed equilateral random walks in 3-space arXiv:1310.5924
- [5] Diao Y, Ernst C, Montemayor A, Rawdon E and Ziegler U 2014 The knot spectrum of confined random equilateral polygons *Mol. Based Math. Biol.* **2** 19–33
- [6] Diao Y, Ernst C, Montemayor A and Ziegler U 2012 Generating equilateral random polygons in confinement II *J. Phys. A: Math. Theor.* **45** 275203

- [7] Diao Y, Ernst C, Montemayor A and Ziegler U 2012 Generating equilateral random polygons in confinement III *J. Phys. A: Math. Theor.* **45** 465003
- [8] Diao Y, Ernst C, Montemayor A and Ziegler U 2013 Curvature of random walks and random polygons in confinement *J. Phys. A: Math. Theor.* **46** 285201
- [9] Diao Y, Ernst C, Montemayor A and Ziegler U 2011 Generating equilateral random polygons in confinement *J. Phys. A: Math. Theor.* **44** 405202
- [10] Jardine P J and Anderson D L 2006 DNA packaging in double-stranded DNA phages *The Bacteriophages* ed R Calendar (Oxford: Oxford University Press) pp 49–65
- [11] Marenduzzo D *et al* 2009 DNA–DNA interactions in bacteriophage capsids are responsible for the observed DNA knotting *Proc. Natl Acad. Sci.* **106** 22269–74
- [12] Millett K C, Rawdon E J, Stasiak A and Sulkowska J I 2013 Identifying knots in proteins *Biochem. Soc. Trans.* **41** 533–7
- [13] Rawdon E J, Millett K C, Sulkowska J I and Stasiak A 2013 Knot localization in proteins *Biochem. Soc. Trans.* **41** 538–41
- [14] Tubiana L, Orlandini E and Micheletti C 2011 Probing the entanglement and locating knots in ring polymers: a comparative study of different arc closure schemes *Prog. Theor. Phys. Suppl.* **191** 192–204
- [15] Zirbel L and Millett K 2012 Characteristics of shape and knotting in ideal rings *J. Phys. A: Math. Theor.* **45** 225001